Automatic detection of wet-snow avalanche seismic signals

Author(s):
Hammer, Conny; Fäh, Donat; Ohrnberger, Matthias

Publication date:
2017-03

Permanent link:
https://doi.org/10.3929/ethz-b-000123562

Originally published in:
Natural Hazards 86(2), https://doi.org/10.1007/s11069-016-2707-0

Nat Hazards (2017) 86:601–618
DOI 10.1007/s11069-016-2707-0

ORIGINAL PAPER

Automatic detection of wet-snow avalanche seismic signals

Conny Hammer[1] · Donat Fäh[1] · Matthias Ohrnberger[2]

Received: 4 June 2015 / Accepted: 26 November 2016 / Published online: 19 December 2016

Abstract Avalanche activity is an important factor when estimating the regional avalanche danger. Moreover, a complete and detailed picture of avalanche activity is needed to understand the processes that lead to natural avalanche release. Currently, information on avalanche activity is mainly obtained through visual observations. However, this involves large uncertainties in the number and release times, influencing the subsequent analysis. Therefore, alternative methods for the remote detection of snow avalanches in particular in non-observed areas are highly desirable. In this study, we use the excited ground vibration to identify avalanches automatically. The specific seismic signature of avalanches facilitates the objective detection by a recently developed classification procedure. A probabilistic description of the signals, called hidden Markov models, allows the robust identification of corresponding signals in the continuous data stream. The procedure is based upon learning a general background model from continuous seismic data. Then, a single reference waveform is used to update an event-specific classifier. Thus, a minimum amount of training data is required by constructing such a classifier on the fly. In this study, we processed five days of continuous data recorded in the Swiss Alps during the avalanche winter 1999. With the restriction of testing large wet-snow avalanches only, the presented approach achieved very convincing results. We successfully detect avalanches over a large volume and distance range. Ninety-two percentage of all detections (43 out of 47) could be confirmed as avalanche events; only four false alarms are reported. We see a clear dependence of recognition capability on run-out distance and source–receiver distance of the observed events: Avalanches are detectable up to a source-receiver distance of eight times the avalanche length. Implications for analyzing a more comprehensive data set (smaller events and different flow regimes) are discussed in detail.

✉ Conny Hammer
conny.hammer@sed.ethz.ch

[1] Swiss Seismological Service, ETH Zürich, Zurich, Switzerland

[2] University of Potsdam, Potsdam, Germany

Keywords Snow avalanche recognition · Automatic detection · Avalanche forecasting · Hidden Markov model

1 Introduction

Detailed information on avalanche activity, i.e., the number and volume of snow avalanches within a specific time and area, is a crucial aspect in a variety of different research areas (e.g., Marienthal et al. 2015; Graveline and Germain 2016). The investigation of potential trigger mechanisms (e.g., Schweizer et al. 2003; Lacroix et al. 2012; Pérez-Guillén et al. 2014), the identification of possible precursors (e.g., Van Herwijnen and Schweizer 2011b; Reiweger and Schweizer 2013; Reiweger et al. 2015) or the determination of return periods (Schweizer et al. 2009) requires a reliable and complete recognition of avalanche events. The reliable identification is also needed at avalanche control sites to measure the effectiveness of the artificial triggering by explosions (Schweizer and van Herwijnen 2013). Moreover, the seismic detection of snow avalanche signals can serve to remove them as "noise," masking other potentially important seismic signals of interest such as earthquakes or man-made explosions (Horasan et al. 2009). Therefore, the remote detection of snow avalanches in particular in non-observed areas is highly desirable. However, most catalogs of snow avalanches are based on visual observations. These catalogs are often incomplete due to a lack of data during low-visibility conditions and have a poor time resolution (Laternser and Schneebeli 2002). Thus, any reliable correlation with potential precursors, trigger mechanisms or meteorological parameters is hardly to find.

Moreover, in alpine regions the reliable recognition of avalanche activity is important for estimating the current avalanche danger. Besides snow pack (e.g., Stoffel et al. 1998; McClung and Schaerer 2006) and (with minor importance) weather (e.g., Ancey et al. 2003; Schweizer et al. 2008; Lacroix et al. 2012) conditions, avalanches are one of the key input parameters for avalanche forecasting. Schweizer and van Herwijnen (2013) showed that the waiting time between avalanches clearly decreases toward peak avalanche activity, suggesting that an early warning based on accurate and near-real-time avalanche activity is possible. However, avalanches occurring at higher altitudes or during nighttimes may go unnoticed for days or weeks by traditional observation techniques. A large number of missed events due to a lack of observations and/or the subjective interpretation of the observer (e.g., regarding the time of avalanche release) affect a correct hazard estimate. Thus, a prerequisite for applying an operational early warning tool is the robust automatic signal detection.

In the past, the identification of snow avalanches has been carried out on a variety of different signal types. Due to regular measurements and the good coverage of satellites, remote sensing enables a comprehensive monitoring of snow avalanches across different spatial scales. Eckerstorfer et al. (2016) give a detailed overview on available remote sensing techniques including respective advantages and limitations. To give but one example, remote sensing photography enables the assessment of avalanche activity with high spatial resolution (Lato et al. 2012). However, its applicability strongly depends on visibility. Recently, Prokop et al. (2013) proposed distributed acoustic fiber optic systems to detect small-sized snow avalanches. In other studies, infrasound has been used to identify snow avalanches (Scott et al. 2006; Ulivieri et al. 2011; Kogelnig et al. 2011b).

Thüring et al. (2015) successfully apply a support vector machine approach to automatically separate noise from small avalanche events in infrasound data.

Besides the described approaches, also the excited ground vibration can be used to identify gravitational mass movements such as debris flows and avalanches (e.g., Leprettre et al. 1998; Marchi et al. 2002; Suriñach et al. 2005; Vilajosana et al. 2008; Deparis et al. 2008; Van Herwijnen et al. 2014). Avalanches are characterized by specific seismic signals (Suriñach et al. 2000; Biescas et al. 2003). Van Herwijnen and Schweizer (2011a) reported that many more avalanches can be detected by seismic monitoring than by visual observation with cameras. However, the manual detection on seismic traces is not feasible since it is extremely costly in terms of time and workload. Setting up an automatic procedure results in a reduced manual workload, and consistent and time-invariant results could be provided for further processing. Moreover, without quasi-real-time automatic avalanche detection, seismic monitoring can hardly be used for operational avalanche forecasting. The seismic detection in real or quasi-real time of snow avalanches would allow timely warnings given to people and would reduce the associated risk.

The use of seismic devices in alpine warning systems is a challenging task (Arattano 1999). Other events such as earthquakes, quarry blasts or man-made noises must be rejected. An approach of progressive elimination of non-avalanche signals is suggested by Leprettre et al. (1996) and further developed by Navarre et al. (2009). Their fuzzy logic rules, defined to see whether a signal was generated by an avalanche event, are based on manual analysis. Hence, a costly preparation of the system is required beforehand. Other systems that are able to automatically detect mass movements such as avalanches, rockfalls or debris flows in an objective way show unsatisfactory results (e.g., Bessason et al. 2007; Arattano and Marchi 2008; Rubin et al. 2012). Bessason et al. (2007) compared observed events (i.e., avalanches, rockfalls, debris flows and earthquakes) to an existing database of more than 300 events using an nearest neighbor approach. However, not more than 74% of all avalanches were identified correctly by the automatic system. Rubin et al. (2012) tested ten different machine learning approaches. In contrast to Bessason et al. (2007), they could detect most of the avalanches (about 90%), but the system reports a large number of false alarms (precision of 13%). Thus, interesting events (i.e., avalanches, debris flows) cannot be identified reliably in an automatic fashion based on their seismic signature resulting in a large number of missed events and/or many false alarms. The reason for this is the classifier, learned from existing waveform samples. Most algorithms require large databases to learn from existing waveform samples. The variability of waveforms, for instance with regard to signal length or frequency content, is generally not captured by the classifier due to a limited number of training events (e.g., Bessason et al. 2007). Especially for observing rare events, this leads to a restricted system performance. Given the former, rather unsatisfying results, there is considerable room for improvement which we begin to fill in this study. The current application does not claim to provide a comprehensive solution but a first step toward robust and complete automatic avalanche identification.

We use a classification procedure based on hidden Markov models (HMM) (Rabiner 1989) to automatically detect large, wet-snow avalanches. As described in similar applications by Hammer et al. (2012, 2013), the advantages are manyfold:

a. Interesting events can be detected automatically in the continuous seismic data stream.
b. Very rare and highly variable signals can be identified successfully.
c. A minimum workload is required to set up the detection and classification system.
d. Detection and classification is carried out in a single step, and no pre- or post-processing is needed.

The method has been tested successfully on a variety of applications, ranging from the automatic identification of volcano seismic signals (Hammer et al. 2012) via the detection of icequakes (Hammer et al. 2015) through to the classification of non-terrestrial signals (Knapmeyer-Endrun and Hammer 2015).

In the next sections, we describe the seismic signature of avalanches followed by an introduction of the analyzed data set. Following this, we explain the classifier and show corresponding results. Finally, we discuss in detail the detection performance including operational considerations.

2 Seismic signature of avalanches

The recorded seismic wavefield of avalanches is complex since the wavefield obtained at the receiver is composed of many phase arrivals. This is due to the moving seismic source and the topography that usually accompanies these phenomena. The seismic signature of snow avalanches is well known and described in several publications (e.g., Suriñach et al. 2000; Biescas et al. 2003; Suriñach et al. 2005). Recently, Pérez-Guillén et al. (2016) showed that different flow regimes cause different seismic signal characteristics. However, independent of flow regime snow avalanches have a smoother beginning than local earthquakes (Fig. 1). The sliding mass is responsible for the characteristic seismic signal. Correspondingly, other mass movements, such as landslides or debris flows, show similar characteristics (Suriñach et al. 2005; Kogelnig et al. 2011a). The material propagation down slope produces a ground vibration. The force transmitted to the ground increases with increasing energy of the avalanche, which depends on its mass and velocity. Any mass increase is converted into an increase in the net force applied to the ground (Suriñach et al. 2005). Therefore, the entrainment of snow during an avalanche release generates signals which increase in amplitude as the mass increases. This characteristic also affects the onset detection. The onset of the seismic signal does not correspond to the avalanche onset, as first a given amount of snow is necessary to generate enough seismic energy to be detected by the sensors (Suriñach et al. 2001). The entrainment of snow also influences the temperature and the humidity of the flowing mass so that the flow regime may change from dry to a denser granular flow (Steinkogler et al. 2014). Different wave trains are due to

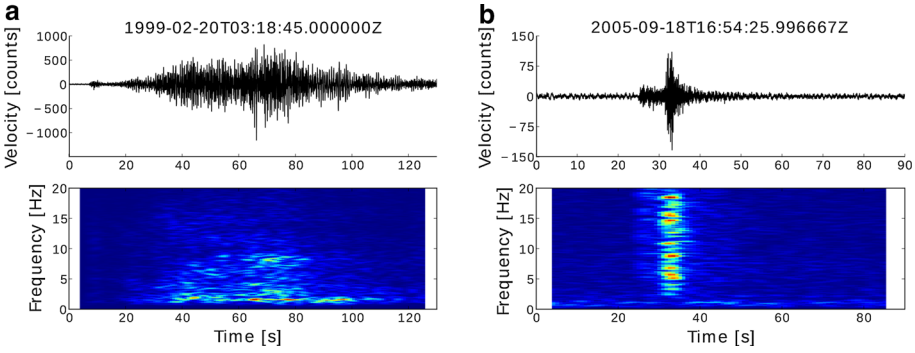

Fig. 1 Waveforms (*top*) and spectrograms (*bottom*) of avalanche (**a**) and local earthquake signal (**b**) recorded at station LLS in the Swiss Alps. The avalanche signal corresponds to event no. 2 in Table 1. Data are bandpass filtered between 1.0 and 30.0 Hz. Window length of fft is 10 s. Note the different time scales in plot (**a**, **b**)

slope changes, interactions with obstacles such as trees or ski lifts and the stopping phase of the avalanche (e.g., Sabot et al. 1998; Suriñach et al. 2000, 2001). Large amplitude peaks in the signal tail are probably related to abrupt mass depositions once the avalanche flow stops suddenly (Pérez-Guillén et al. 2016).

In addition to waveform analysis, the spectral analysis of snow avalanche seismic signals provides several benefits. The overall frequency content can be used to discriminate different avalanche flow regimes (Pérez-Guillén et al. 2016). While wet-snow avalanches generate higher frequencies, powder-snow avalanches are characterized by a lower-frequency content. The difference lies in the distinct flow dynamics. In dense wet-snow avalanches, rapid density and pressure fluctuations generate high-frequency vibrations. In comparison, the low-frequency signals of powder-snow avalanches are due to turbulences in the energetic part of the mass flow (Pérez-Guillén et al. (2016). Independent of flow regime, the spectrograms of avalanches and earthquakes show clear differences (Fig. 1). Snow avalanches are characterized by an increase in frequency content and show a triangular spectrogram (e.g., Suriñach et al. 2001, 2005) which cannot be explained with the Doppler effect (Biescas et al. 2003). The characteristic shape results from a combination of different factors: first, from the frequency-dependent anelastic attenuation of the seismic waves (Suriñach et al. 2005). High frequencies attenuate faster than low frequencies. Therefore, the frequency content increases when the source–receiver distance decreases, i.e., when the avalanche moves toward the recording sensor. The frequency content decreases again after passing the sensor. However, this holds only for the specific case if the receiver is in or at least close to the avalanche path. In addition, the entrainment of snow shapes the spectrogram. The mass increase during the sliding process induces an amplitude increase at all frequencies (Suriñach et al. 2005). Similar observations have been reported for rockfalls and landslides (Suriñach et al. 2005; Jolly et al. 2002). This unique triangular shape unlike many other sources of seismic events in the Swiss Alps (e.g., earthquakes, quarry blasts) suggests that automatic detection and classification is possible. The presented classification approach makes use of this characteristic pattern and successfully detected other mass movements, such as rockfalls, with detection rates of up to 98% (Hammer et al. 2012, 2013; Dammeier et al. 2016).

3 Data set

In this study, we concentrate on the automatic detection of wet-snow avalanches in the Swiss Alps. We processed five days of data recorded during the avalanche winter in 1999 when more than 1300 destructive avalanches took place. We picked this extreme data set to test and tune the new approach extensively for a period of frequent avalanche release. Any implications following the data selection are discussed in the last section. In the following, only a brief overview is given. A detailed description of the avalanche winter is given in Wilhelm et al. (2000). Due to three orographic lifts, three precipitation periods brought large amounts of snow in the Swiss Alps between January 27 and February 25. During these 30 days, the amount of new snow was more than 5 m with most of the snow on the northern flanks of the Alps. The longest precipitation period between February 17 and 25 exhibited the most widespread and longest avalanche cycle known and recorded. The combination of intense snowfalls, strong winds which further accumulated drifted snow and a rising air temperature led to the most intense avalanche activity between February 20 and 23.

In light of the above, we processed five days of continuous data recorded between February 20 and 24. The data were recorded at a broadband station operated by the Swiss Seismological Service (SED). The station Linth–Limmern (LLS) is part of the Swiss Seismological Network and is located on the northern flanks of the Alps in the Canton of Glarus (Fig. 2). Data are recorded with a Streckeisen STS2 broadband sensor and are sampled with a frequency of 120 Hz.

The reference for all avalanches is the avalanche database maintained by the WSL Institute for Snow and Avalanche Research SLF. The database is compiled based on observations. Given this context, not all avalanches are given with an exact release time. Uncertainties up to several hours exist, and for some only the day of release is known. In addition, there might be several missing events. For our study, we considered avalanches within a radius of 30 km around station LLS as test data set. Within this distance range, 19 avalanches are listed with an exact release time. We call these timed avalanches part A of the data set. In addition, 41 avalanches are listed without an exact release time. We call these undetermined events part B of the data set. All events are shown in Fig. 2 and described in Table 1. The avalanche length (the descended path or run-out) ranges from 1170 to 3470 m. That means in terms of the classification scheme proposed by Greene et al. (2010), we deal with avalanche events of size 3, 4 and 5. We estimated the duration of the avalanches as the length of the generated seismic signal recorded at station LLS. The beginning of the signal is defined at the instant when the amplitude starts to stand out from the background noise. Similarly, the end of the signal is defined at the instant when the amplitude is lost in the background noise. Therewith, we obtained signal durations from 43 to 244 seconds. Signals, for which no duration is given in Table 1, are not visible in the seismic data recorded at station LLS (Fig. 3). The data set comprises wet avalanches only.

Example waveforms are shown in Fig. 4. Avalanche (a) is released at a distance of 11.9 km and a backazimuth of 56° from station LLS. In contrast, avalanche (b) is released at a distance of 19.8 km and a backazimuth of 320° from station LLS. Although recorded at different distances and backazimuths, both signals show the typical waveform. The triangular shape of the spectrogram is also present at both signals but much flatter at the

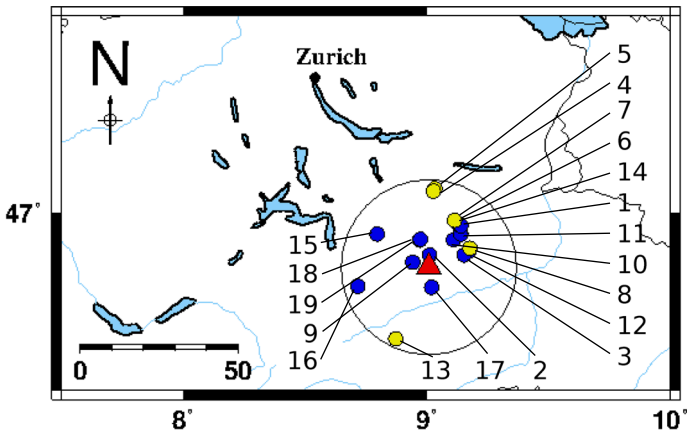

Fig. 2 Location of station LLS in the Alps. The station is indicated by the *red triangle*. The *circle* shows a radius of 30 km around station LLS. Confirmed snow avalanche events that occurred within the given radius between February 20 and 24 are shown. The numbers correspond to avalanche numbers in Table 1. Classification results are *color* coded: <*blue*> detected, <*yellow*> non-detected

Table 1 Snow avalanches given in the SLF database occurred within a radius of 30 km around station LLS between February 20 and 24. Known avalanche locations are shown in Fig. 2. Signals, for which no duration is given, are manually not detectable in the seismic data recorded at station LLS

No	Potential release time (UTC)	Source–receiver distance (km)	Duration (sec)	Run-out distance (m)	RD factor	Detected
Part A, avalanches with exact release time						
1	02.20.1999, 01:00	16.4	45	2500	0.152	Yes
2	02.20.1999, 03:20	4.7	111	2130	0.457	Yes
3	02.20.1999, 07:30	11.5	103	2650	0.230	Yes
4	02.20.1999, 09:30	23.6	–	1900	0.081	No
5	02.20.1999, 10:50	24.6	–	1230	0.050	No
6	02.20.1999, 14:55	18.6	51	2330	0.125	Yes
7	02.20.1999, 17:00	18.8	–	2100	0.112	No
8	02.21.1999, 00:30	14.4	–	1750	0.121	No
9	02.21.1999, 08:00	2.9	202	3300	1.148	Yes
10	02.21.1999, 17:30	11.9	52	3130	0.262	Yes
11	02.21.1999, 20:45	15.7	114	2930	0.187	Yes
12	02.21.1999, 21:30	13.6	244	2320	0.171	Yes
13	02.22.1999, 10:30	25.6	–	1800	0.070	No
14	02.22.1999, 15:45	18.2	69	2050	0.113	Yes
15	02.22.1999, 18:45	19.8	43	2870	0.145	Yes
16	02.23.1999, 06:30	23.7	92	2850	0.120	Yes
17	02.23.1999, 11:50	9.5	52	3470	0.365	Yes
18	02.24.1999, 00:00	7.8	58	1680	0.216	Yes
19	02.24.1999, 00:10	8.1	62	1520	0.188	Yes
Part B, avalanches without exact release time						
20	02.20.1999	18.8		2330	0.124	
21	02.20.1999	7.6		1250	0.165	
22	02.20.1999	18.5		1830	0.099	
23	02.20.1999	18.7		1530	0.082	
24	02.20.1999	18.8		1450	0.077	
25	02.20.1999	28.2		2302	0.082	
26	02.20.1999	29.0		2800	0.097	
27	02.20.1999	29.4		2000	0.068	
28	02.20.1999	30.3		1170	0.039	
29	02.21.1999	11.3		3180	0.281	
30	02.21.1999	27.4		2700	0.098	
31	02.21.1999	27.5		1270	0.046	
32	02.21.1999	28.3		1260	0.045	
33	02.21.1999	28.5		1480	0.052	
34	02.21.1999	29.8		2300	0.077	
35	02.22.1999	20.3		2150	0.106	
36	02.22.1999	25.0		1360	0.054	
37	02.22.1999	10.1		3400	0.336	
38	02.22.1999	13.1		2100	0.160	
39	02.22.1999	16.3		2839	0.174	

Table 1 continued

No	Potential release time (UTC)	Source–receiver distance (km)	Duration (sec)	Run-out distance (m)	RD factor	Detected
40	02.22.1999	18.8		2530	0.135	
41	02.22.1999	19.3		1600	0.083	
42	02.22.1999	20.7		1200	0.058	
43	02.22.1999	21.4		1430	0.067	
44	02.22.1999	26.9		2300	0.085	
45	02.22.1999	27.6		1500	0.054	
46	02.22.1999	27.7		2500	0.090	
47	02.22.1999	28.3		1500	0.053	
48	02.22.1999	29.0		3000	0.103	
49	02.23.1999	28.9		2960	0.102	
50	02.23.1999	24.5		1300	0.053	
51	02.23.1999	25.9		1630	0.063	
52	02.23.1999	26.0		1580	0.061	
53	02.23.1999	27.4		1700	0.062	
54	02.23.1999	29.5		1300	0.044	
55	02.23.1999	29.8		2300	0.077	
56	02.24.1999	18.0		2700	0.150	
57	02.24.1999	7.4		2130	0.290	
58	02.24.1999	12.3		1750	0.142	
59	02.24.1999	24.4		1970	0.081	
60	02.24.1999	29.2		3500	0.120	

more distant one. Due to large source–receiver distances, the triangular spectral shape cannot be caused by anelastic attenuation as described in the previous section. Instead, solely the entrainment of snow seems to provoke this characteristic shape.

4 Methods

Most of the proposed methods for automatic seismic detection of snow avalanches suffer from an inappropriate classifier. Often, the variability inherent in each signal class is not captured by the corresponding classifier. This leads to a large number of false alarms and/or missed events (e.g., Bessason et al. 2007; Rubin et al. 2012). To overcome this problem, we will use a novel automatic event spotting procedure based on HMMs. The proposed technique was developed for the volcanic task force action where a robust system that can be set up quickly is of great importance (Hammer et al. 2012). In the following, we give only a very brief description of the used approach. A detailed description is given in Hammer et al. (2012) and Hammer et al. (2013) for the detection of volcanic signals, quarry blasts and earthquakes. We keep the basic procedure presented in those former studies for the current application. Only the window length for feature computation is adjusted as explained below.

The classification approach is not based on the seismic waveform directly but on specific attributes extracted from the continuous waveform. Hence, the raw waveform is

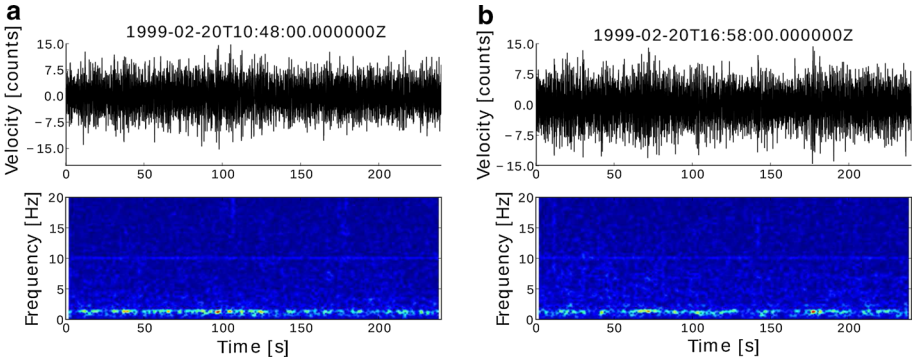

Fig. 3 Waveforms (*top*) and spectrograms (*bottom*) of avalanches not visible at station LLS. Signals correspond to events no. 5 (**a**) and 7 (**b**) in Table 1. Data are bandpass filtered between 1.0 and 30.0 Hz. Window length of fft is 5 s

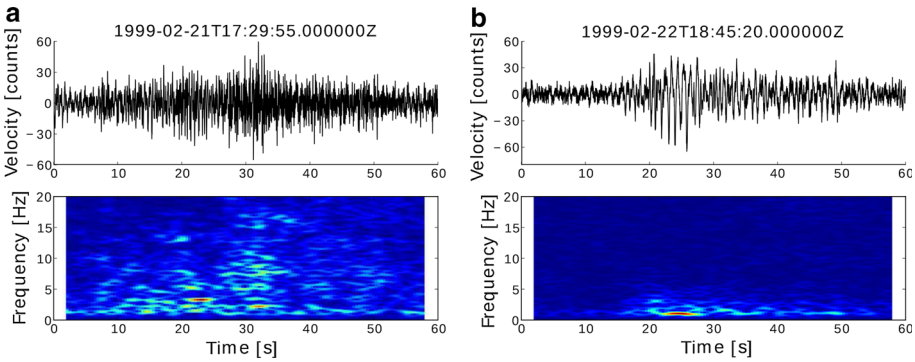

Fig. 4 Waveforms (*top*) and spectrograms (*bottom*) of avalanches at different distances from the station LLS. The source–receiver distance is (**a**) 11.9 km and (**b**) 19.8 km. Signals correspond to events no. 10 (**a**) and 15 (**b**) in Table 1. Data are bandpass filtered between 1.0 and 30.0 Hz. Window length of fft is 5 s

replaced by a sequence of feature vectors (i.e., short-term wavefield attributes). In that way, redundant information diminishes and the waveforms are reduced to the substantial information which is relevant for discriminating different seismic signal classes. Then, for each signal class of interest a HMM is constructed from available training data. That means, the feature pattern, characteristic for a specific signal class, is modeled by a sequence of Gaussian probability distributions (Fig. 5). Using distributions rather than fixed values allows for a certain variability of the typical event pattern. Within an event, each distribution is active for a specific time interval. This duration is also given in a probabilistic fashion, allowing the active interval to vary within a specific time range. Thus, the signal can be compressed or stretched along the time axis. The approach is illustrated in Fig. 5.

The parameters defining each HMM (i.e., means and variances of Gaussians as well as residence time for each Gaussian) are learned from pre-classified training data. While the classical learning approach requires a large amount of training data, here we use a training procedure recently developed. The procedure is based upon learning a general background model from a continuous seismic data stream. Then, a single reference waveform is used to

update an event class-specific classifier. In that way, a minimum amount of training data is required by constructing such a classifier on the fly while enabling the recognition of highly variable time series. Sparse training data, which do not contain existing waveform variability, lead to a restricted system performance for most classification methods. Our algorithm overcomes this problem by enabling the reliable automatic detection of rare and highly variable events.

In the current study, the description above translates to the following work procedure. First a set of appropriate features is chosen to discriminate the seismic signal produced by avalanches from other seismic sources such as earthquakes or ambient noise. Given the triangular shape of the spectrogram, spectral attributes seem most appropriate for this task. Thus, we extracted the energy in seven half-octave bands ranging from 1 to 15 Hz, the central frequency, the instantaneous frequency, the instantaneous bandwidth, the first three cepstral coefficients and the largest eigenvalue from corresponding events (a detailed description of these features can be found in Hammer et al. (2012)). The window length for feature computation is 256 samples (approximately 2.13 seconds), and the window is shifted with a step size of 0.25 s over the continuous data stream. While window length is the same as used before for detecting earthquakes and quarry blasts at SED stations, the step size is much larger (Hammer et al. 2013). The long event duration of avalanches compared to local earthquakes or quarry blasts allows to use much larger step sizes. As a result, typical characteristics are preserved, while feature time series are much smoother. After feature computation, a background model, which captures all non-interesting signals, is constructed from four hours of continuous recording. Together with this general wavefield description and an appropriate reference signal (Fig. 1a), an avalanche HMM is then build immediately. In order to reduce the number of spurious detections, a minimum

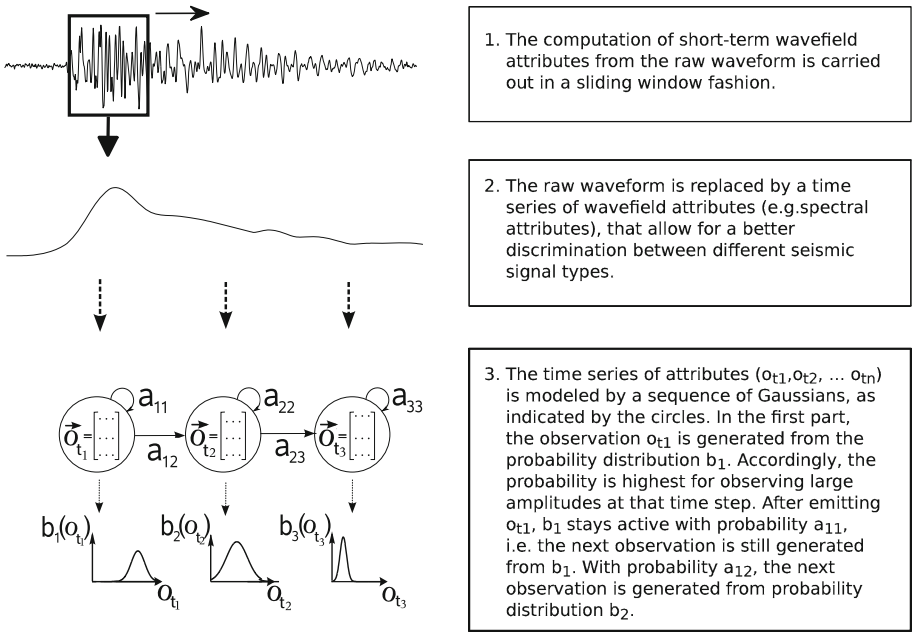

Fig. 5 Sketch of the construction of an event HMM

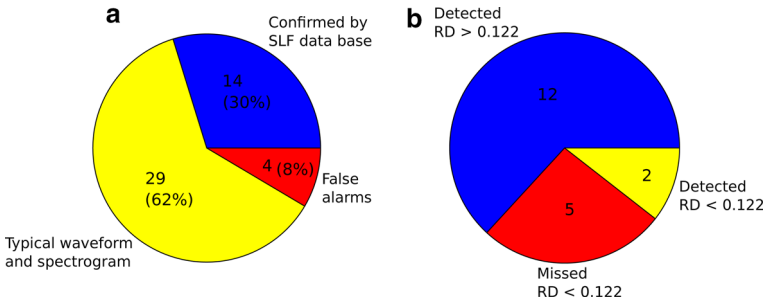

Fig. 6 Pie diagram of detections. **a** All detections given by the automatic system. Of these 30% correspond to events given in the SLF database <*blue*>, 62% are validated by typical waveforms and spectrograms <*yellow*> and 8% are false alarms <*red*>. **b** Avalanche events given in data set A. All avalanches showing RD > 0.122 (12 in number) are detected <*blue*>. Two avalanches with RD < 0.122 are detected <*yellow*>. Five avalanches with RD < 0.122 are not detectable <*red*>

length of 10 s is required for a valid detection. All detections with a duration shorter than 10 s are rejected.

As noted by Biescas et al. (2003), we expect the detection capability to have a natural limit which depends on the distance between seismometer and avalanche and the mass involved. With increasing source–receiver distance, signals are attenuated at an increasing rate and the larger the avalanche, the larger the net force that is applied to the ground. In this study, we have no information on the size of considered avalanches. For that reason, we use the run-out distance as a proxy for the avalanche size. We define the recognition discriminant (RD)

$$\mathrm{RD} = \frac{\text{run}-\text{out distance [m]}}{\text{source}-\text{receiver distance [m]}} \tag{1}$$

to describe the dependency of recognition capability and avalanche parameters in detail. In the next section, we analyze obtained results with regard to corresponding RD values.

5 Results

The defined test data set of avalanches is given in Table 1. In the radius of 30 km around station LLS, 19 avalanches with exact release times are listed in the SLF database (part A in Table 1). In addition, 41 avalanches are listed without an exact release time (part B in Table 1).

Overall, 47 detections are reported by the automatic system (Fig. 6a). In order to evaluate this result, the detections can be categorized in two groups: events that can be matched with listed avalanches and those which cannot. Since the release times are known, the detections can be only compared with part A of the data set. Fourteen detections correspond to avalanche events in data set A (i.e., 14 out of 19 timed events are detected, Fig. 6b). For the remaining 33 detections, no field observations are available. These signals might either be among confirmed events with unknown release time (data set B in Table 1), might belong to non-observed avalanches or might be false alarms. Considering the specific seismic signature described in Sect. 4, we investigated these 33 detections in detail. Twenty-nine out of 33 detections show the typical triangular shape of the

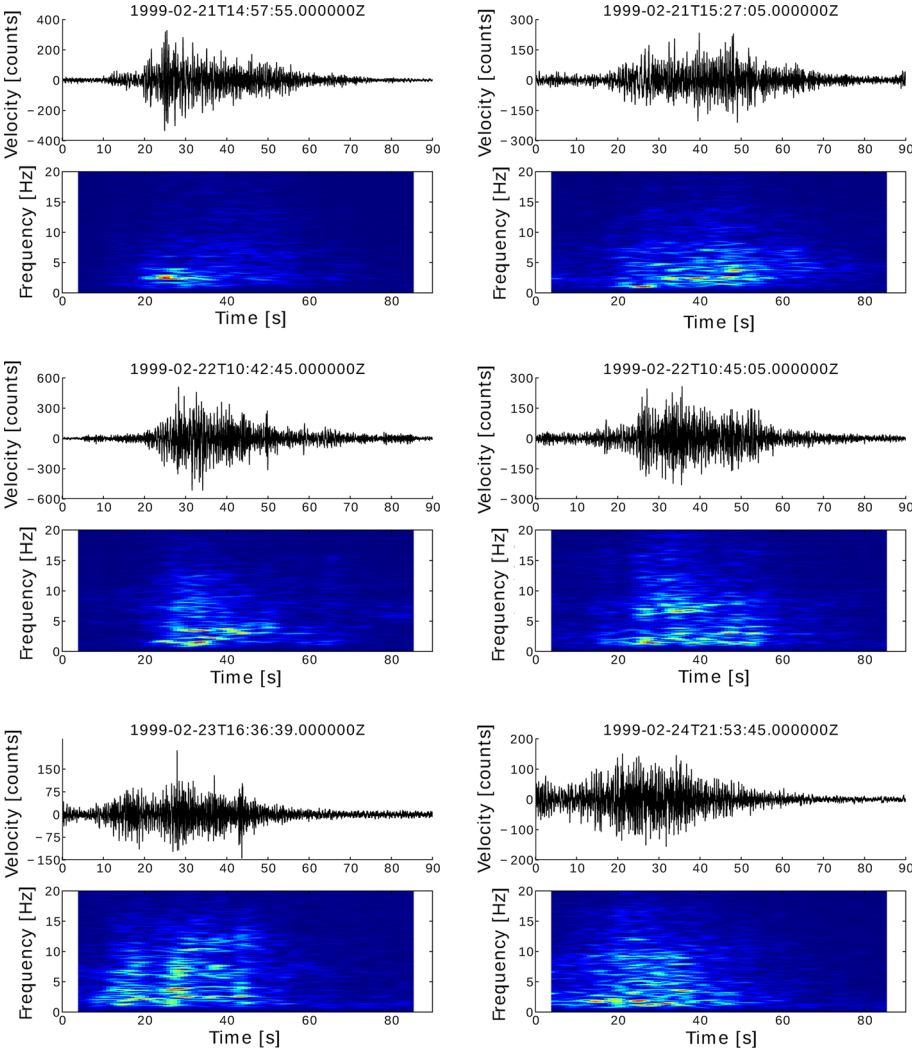

Fig. 7 Example waveforms and spectrograms of events that are identified as avalanche signal by the automatic system and can be confirmed by manual investigation. Signals might correspond to avalanches in data set B in Table 1 or might belong to non-observed avalanches. Data are bandpass filtered between 1.0 and 30.0 Hz. Window length of fft is 10 s

spectrogram and the typical waveform. Some examples are given in Fig. 7. Based on our manual analysis of spectrogram and waveform, we conclude that 29 detections correspond to true avalanche releases. The remaining four detections cannot be confirmed to be avalanches by the seismic waveform and/or the corresponding spectrogram (Fig. 8). All four events are shorter than typical avalanche events. Especially, the events in Fig. 8a and d do not show a triangular spectrogram, but a rather monochromatic frequency content. Hence, we declared them as false alarms.

Fourteen out of 19 confirmed avalanches are detected by the automatic classifier. Five avalanche events are not detected. It should be noted that none of the five events is

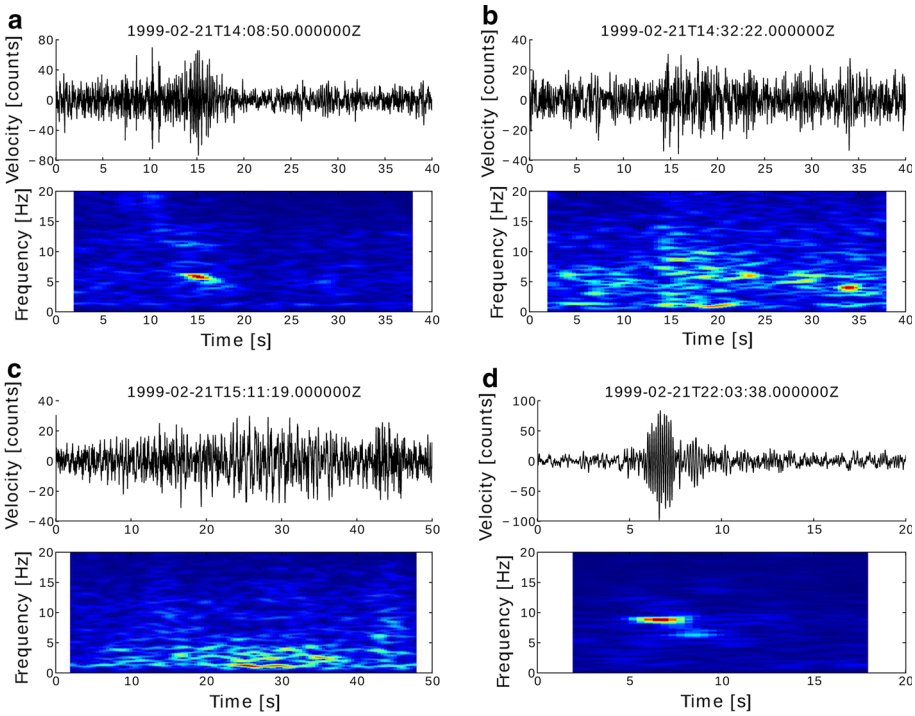

Fig. 8 Waveforms and spectrograms of events that are recognized as avalanche signal by the automatic system but are identified as false alarms in the manual investigation. Data are bandpass filtered between 1.0 and 30.0 Hz. Window length of fft is 5 s

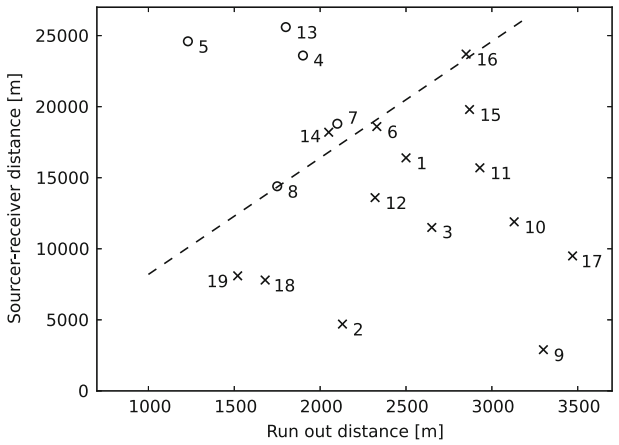

Fig. 9 Run-out distance and source–receiver distance of detected $< \times >$ and non-detectable $< \circ >$ events. The *dashed line* corresponds to RD= 0.122. Numbers correspond to avalanche numbers in Table 1

manually identifiable on the seismic data at the assigned time. Given that the non-detectable avalanches are characterized by a small run-out length or by a large source–receiver distance (events no. 4, 5, 7, 8 and 13 in Table 1), we investigate this dependency

in detail. Figure 9 shows run-out distance and source–receiver distance of detected and non-detected events. There is a clear link between both parameters and the outcome of the automatic detection system. The smaller the source–receiver distance, the smaller the size of avalanches that are detectable. All non-detected avalanches are characterized by RD <0.122. Except two, all successful detections are characterized by RD > 0.122. The exception here is two avalanches that are successfully detected but show a low RD of 0.113 and 0.120 (events no. 14 and 16 in Table 1).

6 Discussion and conclusion

The presented approach shows very promising detections results. For 19 avalanche events, field evidence is available. All visible avalanches within a source–receiver distance range of 30 km are detected successfully (14 in number). Although events show significant differences in their waveforms and spectrograms (Fig. 4), the stochastic approach of hidden Markov models allows the detection of events over a large volume (run-out 1.0–3.5 km), duration (43–244 s) and source–receiver distance (3–25 km) range. While the prototype is build from an event that occurred close to station LLS (Fig. 1a), events at a distance of up to 25 km are successfully identified by the automatic system. Five events are not detected as amplitudes are too small and disappear in the background noise. The reason for this is attenuation, which increases with increasing distance. Moreover, detection capability depends on the size of the avalanche as already reported by Biescas et al. (2003). We found a limit of the detection capability conditioned on avalanche size (defined indirectly by the run-out distance) and source–receiver distance. All avalanches with RD > 0.122 are detected successfully. In addition, two events with lower RD factor are also identified. The reason for this might be the use of run-out distance as a proxy for volume. Other parameters such as slope angle or type of avalanche also influence the avalanche length. Moreover, there might be a general transition zone between detectable and non-detectable events where values of RD vary within a certain range. The detection performance for avalanches within this zone is more sensitive to external parameters such as the local noise level or snow conditions and may change from day to day.

The results above allow to draw conclusions about the potential detection distance with regard to avalanche size. The value of RD > 0.122 translates to the following rough estimate: Avalanches are detectable up to a source–receiver distance of eight times the avalanche length. This gives a detection radius of 0.4 to 4.1 km for avalanches with a smaller run-out of 50–500 m. The permanent Swiss seismic broadband network has an average inter-station distance of 30 km. Consequently, avalanches having a run-out of more than 1800 m could be identified at least on one station if the algorithm were running on the complete network. Moreover, in some specific regions the station density in Switzerland is much higher. In the canton of Valais, the inter-station distance is 10 km on average. That decreases the minimum detectable avalanche run-out size to 600 m. For process investigations, often small temporal networks are installed. Station distances of less than 500 m are common; thus, much smaller avalanches can be detected. Finally, it should be noted that we expect deviations from the proposed limit of RD $= 0.122$ for source–receiver distances close zero as a certain amount of snow is necessary to generate enough ground vibration to be recorded by the sensors.

Additionally to the avalanches in data part A, the system detected 33 avalanches. Twenty-nine detections could be confirmed by visually verifying the automatically

obtained classifications. Four false alarms were declared. However, given the manual evaluation process, it cannot ruled out that there are flaws in the manually assigned labels. Most of the events listed in data part B have an RD value below 0.122 (Table 1). Based on our results yielded from the analysis of RD, we assume that they are not detected by the automatic system. Consequently, the system detected avalanches not listed in the SLF database due to incomplete observations.

The reasons for the four false alarms are not clear. While two signals (Fig. 8a, d) are most likely caused by pumps close to station LLS, the other two are not easily defined. In addition, there is no straightforward explanation for the results of the HMM-based detection approach. The selected parametrization is based on time patterns of a set of short-term wavefield attributes. The only conclusion to be drawn is that the seismic wavefield attributes of these four events share significantly more similarities to the seismic wavefield characteristics recorded for avalanches if compared to the characteristics of seismic noise.

Above results summarize to an overall precision of 92% within $RD > 0.122$. However, we have to admit that the high success rate might be the result of the events used in this study. During the considered observation period, only large, wet avalanches took place. We are aware of the fact that this data selection provides a significant restriction. As regards size, all events have a run-out of more than one kilometer, which classifies them as size 3, 4 or 5 avalanches. As for the flow regime, all events are characterized as wet avalanches. However, most avalanches that occur during a winter season have a run-out of less than 500 m. In addition, different kinds of avalanche flow regimes might have a different seismic signature. Due to higher masses and better acoustic coupling to the ground, wet avalanches might produce signals with higher amplitudes than dry ones. Moreover, in the exceptional avalanche period we are considering, the snow cover might affect attenuation (Pérez-Guillén et al. 2016) influencing the classifier performance. Finally, all events were observed during a short time period of five days where signal propagation properties and background noise might not vary much. However, we picked this data set to test the new approach extensively for a period of frequent avalanche release. In addition, we wanted to apply the algorithm to a single broadband station, investigating the gain for existing seismic networks. In order to meet both requirements, we choose the corresponding data set.

In order to evaluate the local avalanche danger or to understand corresponding processes, avalanche forecasting services are interested in a complete overview of avalanche activity. Although the application does not analyze a comprehensive avalanche data set, it shows an encouraging path for future research. Especially in combination with results from other studies, the current approach seems promising. Using the presented algorithm, Dammeier et al. (2016) automatically identified rockfalls over a large volume and distance range. Although signals do not always show similar properties, they can be detected successfully due to the stochastic approach of HMMs. Furthermore, Suriñach et al. (2005) show that the triangular spectrogram is a general and independent feature regardless of type of avalanche (e.g., wet/dry). The spectral shape is modeled by the corresponding HMM and a key parameter to distinguish avalanches from other sources. Thus, a successful automatic detection of non-wet avalanches seems very likely. Potential noise variations occurring during a longer observation period can be accounted for by retraining the background model on a regular basis of days or even hours (e.g., Hammer et al. 2015; Dammeier et al. 2016). Similarly, substantial changes in avalanche signal characteristics or propagation properties can be included by constructing new event models. This can be done immediately after a single example of the new event class has been recorded.

In this study, the detection is carried out at the vertical component of a single station of the Swiss broadband network. The obtained results imply that a single station or geophone may be a practicable and inexpensive option to identify avalanches within a specific region. But the performance would also gain from setting up the system at a small network. First, the number of false alarms might be further reduced by combining detection results of several stations. Second, it would be possible to locate the avalanche events, which would be of great importance for an operational setup.

Biescas et al. (2003) report on different detection performances for different types of flow regimes. In this study, we did consider only large wet avalanches. The application of the proposed method to small, powder avalanches will be subject to future research. In addition, this opens up another challenge. Given an unknown avalanche size and distance, wet and powder avalanches cannot be distinguished by seismic detection only. However, Kogelnig et al. (2011b) showed that a combination of infrasound and seismic sensors allowed to detect different avalanche regimes. Following this, the joint setup of different kinds of sensors might be a beneficial direction for future research.

Acknowledgements This work was partly funded by the project Swiss Experiment, funded by the Competence Center for Environment and Sustainability of the ETH Domain (CCES). We thank Jürg Schweizer from SLF for providing detailed information on avalanches used in this study.

References

Ancey C, Meunier M, Richard D (2003) Inverse problem in avalanche dynamics models. Water Resour Res 39(4):1099. doi:10.1029/2002WR001749

Arattano M (1999) On the use of seismic detectors as monitoring and warning systems for debris flows. Nat Hazards 20(2–3):197–213. doi:10.1023/A:1008061916445

Arattano M, Marchi L (2008) Systems and sensors for debris-flow monitoring and warning. Sensors 8(4):2436–2452. doi:10.3390/s8042436

Bessason B, Eiriksson G, Thorarinsson O, Thorarinsson A, Einarsson S (2007) Automatic detection of avalanches and debris flows by seismic methods. J Glaciol 53(182):461–472. doi:10.3189/002214307783258468

Biescas B, Dufour F, Furdada G, Khazaradze G, Suriñach E (2003) Frequency content evolution of snow avalanche seismic signals. Surv Geophys 24(5–6):447–464. doi:10.1023/B:GEOP.0000006076.38174.31

Dammeier F, Moore JR, Hammer C, Haslinger F, Loew S (2016) Automatic detection of alpine rockslides in continuous seismic data using hidden Markov models. J Geophys Res Earth Surf 121(2):351–371. doi:10.1002/2015JF003647

Deparis J, Jongmans D, Cotton F, Baillet L, Thouvenot F, Hantz D (2008) Analysis of rock-fall and rock-fall avalanche seismograms in the French Alps. Bull Seismol Soc Am 98(4):1781–1796. doi:10.1785/0120070082

Eckerstorfer M, Bühler Y, Frauenfelder R, Malnes E (2016) Remote sensing of snow avalanches: recent advances, potential, and limitations. Cold Reg Sci Technol 121:126–140. doi:10.1016/j.coldregions.2015.11.001

Graveline MH, Germain D (2016) Ice-block fall and snow avalanche hazards in northern Gaspesie (eastern Canada): triggering weather scenarios and process interactions. Cold Reg Sci Technol 123:81–90. doi:10.1016/j.coldregions.2015.11.012

Greene E, Atkins D, Birkeland K, Elder K, LAndry C, Lazar B, McCammon I, Moore M, Sharaf D, Sterbenz C, Tremper B, Williams K (2010) Snow, weather and avalanches: observational guidelines for avalanche programs in the United States. American Avalanche Association (AAA) Pagosa Springs.

Hammer C, Beyreuther M, Ohrnberger M (2012) A seismic-event spotting system for volcano fast-response systems. Bull Seismol Soc Am 102(3):948–960. doi:10.1785/0120110167

Hammer C, Ohrnberger M, Faeh D (2013) Classifying seismic waveforms from scratch: a case study in the alpine environment. Geophys J Int 192(1):425–439. doi:10.1093/gji/ggs036

Hammer C, Ohrnberger M, Schlindwein V (2015) Pattern of cryospheric seismic events observed at Ekström Ice Shelf, Antarctica. Geophys Res Lett 42(10):3936–3943. doi:10.1002/2015GL064029

Horasan G, Guney AB, Kusmezer A, Bekler F, Ogutcu Z, Musaoglu N (2009) Contamination of seismicity catalogs by quarry blasts: an example from Istanbul and its vicinity, northwestern Turkey. J Asian Earth Sci 34(1):90–99. doi:10.1016/j.jseaes.2008.03.012

Jolly AD, Thompson G, Norton GE (2002) Locating pyroclastic flows on Soufriere Hills Volcano, Montserrat, West Indies, using amplitude signals from high dynamic range instruments. J Vol Geotherm Res 118(3):299–317. doi:10.1016/S0377-0273(02)00299-8

Knapmeyer-Endrun B, Hammer C (2015) Identification of new events in Apollo 16 lunar seismic data by Hidden Markov Model-based event detection and classification. J Geophys Res Planets 120(10):1620–1645. doi:10.1002/2015JE004862

Kogelnig A, Hübl J, Suriñach E, Vilajosana I, McArdell B (2011a) Infrasound produced by debris flow: propagation and frequency content evolution. Nat Hazards 70(3):1713–1733. doi:10.1007/s11069-011-9741-8

Kogelnig A, Suriñach E, Vilajosana I, Hübl J, Sovilla B, Hiller M, Dufour F (2011) On the complementariness of infrasound and seismic sensors for monitoring snow avalanches. Nat Hazards Earth Syst Sci 11(8):2355–2370. doi:10.5194/nhess-11-2355-2011

Lacroix P, Grasso JR, Roulle J, Giraud G, Goetz D, Morin S, Helmstetter A (2012) Monitoring of snow avalanches using a seismic array: Location, speed estimation, and relationships to meteorological variables. J Geophys Res Earth Surf 117, F01034. doi:10.1029/2011JF002106

Laternser M, Schneebeli M (2002) Temporal trend and spatial distribution of avalanche activity during the last 50 years in Switzerland. Nat Hazards 27(3):201–230. doi:10.1023/A:1020327312719

Lato MJ, Frauenfelder R, Bühler Y (2012) Automated detection of snow avalanche deposits: segmentation and classification of optical remote sensing imagery. Nat Hazards Earth Syst Sci 12(9):2893–2906. doi:10.5194/nhess-12-2893-2012

Leprettre B, Navarre J, Taillefer A (1996) First results from a pre-operational system for automatic detection and recognition of seismic signals associated with avalanches. J Glaciol 42(141):352–363. doi:10.3198/1996JoG42-141-352-363

Leprettre B, Martin N, Glangeaud F, Navarre JP (1998) Three-component signal recognition using time, time-frequency, and polarization information-application to seismic detection of avalanches. IEEE Trans Signal Process 461:83–102. doi:10.1109/78.651183

Marchi L, Arattano M, Deganutti A (2002) Ten years of debris-flow monitoring in the Moscardo Torrent (Italian Alps). Geomorphology 46(1–2):1–17. doi:10.1016/S0169-555X(01)00162-3

Marienthal A, Hendrikx J, Birkeland K, Irvine KM (2015) Meteorological variables to aid forecasting deep slab avalanches on persistent weak layers. Cold Reg Sci Technol 120(SI):227–236. doi:10.1016/j.coldregions.2015.08.007

McClung DM, Schaerer P (2006) The avalanche handbook. The Mountaineers Books, Seattle

Navarre JP, Bourova E, Roulle J, Deliot Y (2009) The seismic detection of avalanches: an information tool for the avalanche forecaster. In: International snow science workshop. International Snow Science Workshop, Davos, Switzerland, SEP 27–OCT 02, pp 379–383

Pérez-Guillén C, Tapia M, Furdada G, Suriñach E, McElwaine JN, Steinkogler W, Hiller M (2014) Evaluation of a snow avalanche possibly triggered by a local earthquake at Vallee de la Sionne, Switzerland. Cold Reg Sci Technol 108:149–162. doi: 10.1016/j.coldregions.2014.07.007

Pérez-Guillén C, Sovilla B, Suriñach E, Tapia M, Köhler A (2016). Deducing avalanche size and flow regimes from seismic measurements. Cold Reg Sci Technol 121:25–41. doi:10.1016/j.coldregions.2015.10.004

Prokop A, Wirbel A, Jungmayr M (2013) The avalanche detector–a new avalanche monitoring tool using distributed acoustic fibre optic sensing. In: International snow science workshop, International Snow Science Workshop, Grenoble Chamonix Mont-Blanc, France, pp. 458–462

Rabiner L (1989) A tutorial on hidden markov-models and selected applications in speech recognition. Proc IEEE 77(2):257–286

Reiweger I, Schweizer J (2013) Measuring acoustic emissions in an avalanche starting zone to monitor snow stability. In: International snow science workshop, International Snow Science Workshop, Grenoble Chamonix Mont-Blanc, France, pp. 942–944

Reiweger I, Mayer K, Steiner K, Dual J, Schweizer J (2015) Measuring and localizing acoustic emission events in snow prior to fracture. Cold Reg Sci Technol 110:160–169. doi:10.1016/j.coldregions.2014.12,002

Rubin MJ, Camp T, Herwijnen AV, Schweizer J (2012) Automatically detecting avalanche events in passive seismic data. In: Proceedings of the 2012 11th international conference on machine learning and applications, vol. 1. ICMLA '12, pp 13–20. doi:10.1109/ICMLA.2012.12

Sabot F, Naaim M, Granada F, Suriñach E, Planet P, Furdada G (1998) Study of avalanche dynamics by seismic methods, image-processing techniques and numerical models. Ann Glaciol 26:319–323. doi:10.3198/1998AoG26-1-319-323

Schweizer J, van Herwijnen A (2013) Can near real-time avalanche occurrence data improve avalanche forecasting? In: International snow science workshop. International Snow Science Workshop, Grenoble Chamonix Mont-Blanc, France, 2013, pp. 195–198

Schweizer J, Jamieson B, Schneebeli M (2003) Snow avalanche formation. Rev Geophys 41(4):1944–9208. doi:10.1029/2002RG000123

Schweizer J, Mitterer C, Stoffel L (2008) Determining the critical new snow depth for a destructive avalanche by considering the return period. In: International snow science workshop, International Snow Science Workshop, Whistler, Canada, SEP 21-26, pp. 292–298

Schweizer J, Mitterer C, Stoffel L (2009) On forecasting large and infrequent snow avalanches. Cold Reg Sci Technol 59(2–3, SI):234–241. doi:10.1016/j.coldregions.2009.01.006

Scott ED, Hayward CT, Colgan TJ, Hamann JC, Fubichek RF, Pierre JW, Yount J (2006) Practical implementation of avalanche infrasound monitoring technology for operational utilization near teton pass wyoming. In: International snow science workshop

Steinkogler W, Sovilla B, Lehning M (2014) Influence of snow cover properties on avalanche dynamics. Cold Reg Sci Technol 97:121–131. doi:10.1016/j.coldregions.2013.10.002

Stoffel A, Meister R, Schweizer J (1998) Spatial characteristics of avalanche activity in an alpine valley-a gis approach. Ann Glaciol 26:329–336. doi:10.3198/1998AoG26-1-329-336

Suriñach E, Furdada G, Sabot F, Biescas B, Vilaplana J (2001) On the characterization of seismic signals generated by snow avalanches for monitoring purposes. Ann Glaciol 32:268–274. doi:10.3189/172756401781819634

Suriñach E, Sabot F, Furdada G, Vilaplana J (2000) Study of seismic signals of artificially released snow avalanches for monitoring purposes. Phys Chem Earth Part B Hydrol Oceans Atmos 25(9):721–727. doi:10.1016/S1464-1909(00)00092-7

Suriñach E, Vilajosana I, Khazaradze G, Biescas B, Furdada G, Vilaplana JM (2005) Seismic detection and characterization of landslides and other mass movements. Nat Hazards Earth Syst Sci 5(6):791–798. doi:10.5194/nhess-5-791-2005

Thüring T, Schoch M, van Herwijnen A, Schweizer J (2015) Robust snow avalanche detection using supervised machine learning with infrasonic sensor arrays. Cold Reg Sci Technol 111:60–66. doi:10.1016/j.coldregions.2014.12.014

Ulivieri G, Marchetti E, Ripepe M, Chiambretti I, Da Rosa G, Segor V (2011) Monitoring snow avalanches in Northwestern Italian Alps using an infrasound array. Cold Reg Sci Technol 69(2–3, SI):177–183. doi:10.1016/j.coldregions.2011.09.006

Valt M, Pesaresi D (2009) Detecting snow avalanches with seismic stations in North-east Italy: first results of dataset analysis. In: International snow and science workshop, International Snow Science Workshop, Davos, Switzerland, SEP 27-OCT 02, pp. 458–462

Van Herwijnen A, Schweizer J (2011) Monitoring avalanche activity using a seismic sensor. Cold Reg Sci Technol 69(2–3, SI):165–176. doi:10.1016/j.coldregions.2011.06.008

Van Herwijnen A, Schweizer J (2011b) Seismic sensor array for monitoring an avalanche start zone: design, deployment and preliminary results. J Glaciol 57(202):267–276. doi:10.3189/002214311796405933

Van Herwijnen A, Heck M, Schweizer J (2014) Detecting avalanches using seismic monitoring systems. In: International snow science workshop. International Snow Science Workshop, Banff, pp 116–121

Vilajosana I, Suriñach E, Abellan A, Khazaradze G, Garcia D, Llosa J (2008) Rockfall induced seismic signals: case study in Montserrat, Catalonia. Nat Hazards Earth Syst Sci 8(4):805–812. doi:10.5194/nhess-8-805-2008

Wilhelm C, Wiesinger T, Brundl M, Ammann W (2000) The avalanche winter 1999 in Switzerland – an Overview. In: International snow science workshop, pp. 487–494